THE JOURNAL OF PHYSICAL CHEMISTRY C

Article

pubs.acs.org/JPCC

In Situ Ultralow-Frequency Raman Tracking of the Polymorphic Transformation of Crystalline 1,1′-Binaphthyl

Chun-Fu Chang, Szu-Cheng Wang, and Shinsuke Shigeto*

Department of Applied Chemistry, National Chiao Tung University, Hsinchu 30010, Taiwan

Supporting Information

ABSTRACT: Extremely low-frequency (LF) Raman spectroscopy that allows for fast access to lattice vibrations with little hindrance of immense Rayleigh scattering was used to track in situ thermally induced polymorphic transformation of crystalline 1,1′-binaphthyl (BN), a fundamental structural unit of specific chiral ligands. BN occurs in two conformational polymorphs, cisoid and transoid forms, with the former being a racemate and the latter being a conglomerate of chiral crystals. Observed LF Raman spectra (from 200 cm^{-1} down to ∼5 cm^{-1}, equivalent to 0.15 THz), which arise predominantly from lattice vibrations, show markedly different features between the cisoid and transoid forms, making it possible to study their phase transition. A series of LF Raman spectra measured with slow heating of microcrystalline BN reveal that, in contrast to previous studies, the monoclinic cisoid form transforms directly to the tetragonal transoid form in the solid state without formation of any intermediate phase. The present approach is applicable to various phase transition systems, including pharmaceutical compounds, liquid crystals, and polymer films, which conventional X-ray diffraction analysis may not be able to investigate.

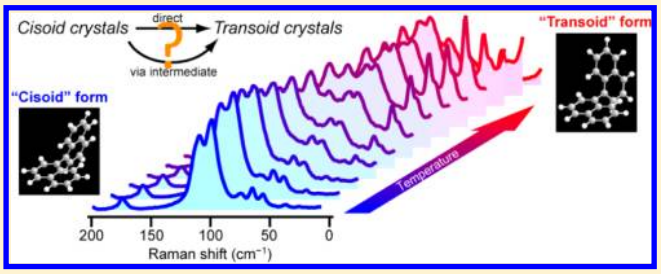

INTRODUCTION

Molecular crystals often exhibit more than one structure that has different three-dimensional arrangements and/or conformations of the constituent molecules in the crystal lattice. This phenomenon termed crystal polymorphism has been arousing keen interest in medicinal chemistry[1,2] as well as in materials science and crystal engineering.[3−5] Because the physical and chemical properties of crystal polymorphs can vary drastically from one form to another, it is imperative in the pharmaceutical industry, for example, to understand and ultimately control the polymorphism of a given active pharmaceutical ingredient. Polymorphism is also relevant to the chemistry of allotropes, perhaps the most important of which are those of carbons[6] (carbon nanotubes, fullerenes, and graphene).

One of the challenges in crystal polymorph control is transformations between different crystal forms. Polymorphic transformation is a type of phase transition occurring in response to various external physical stresses, such as heating, milling, and so on.[1] Many molecular crystals, particularly those that are composed of conformationally flexible molecules (i.e., conformational polymorphs[7]), are known to undergo transformations, which tend to substantially affect their physicochemical properties. The molecular mechanisms for polymorphic transformations are therefore of great importance for a better understanding of these dynamic processes. Commonly employed X-ray diffraction can obtain precise atomic arrangements in crystals but suffers from many restrictions in its wide application to the transformation dynamics.

Here we use ultralow-frequency Raman spectroscopy to track the polymorphic transformation of crystalline 1,1′-binaphthyl (BN) in situ. Our apparatus that combines an iodine vapor cell[8−12] as an ultranarrow notch filter with a state-of-the-art multichannel detector can measure Raman spectra in the extremely low-frequency (LF) region (∼5 to 200 cm^{-1}), which is not accessible with the ordinary Raman spectrometer. Because LF Raman spectra convey a wealth of information on collective lattice vibrations of crystals, they are far more sensitive to differences in crystal structure than normally recorded high-frequency (HF) Raman spectra,[13] thus making feasible in situ molecular-level tracking of polymorphic transformations.

BN is a typical biaryl compound that has been the subject of extensive studies in the condensed phase[14−21] as well as in the gas phase.[22] It occurs as two distinct crystal forms. This polymorphism is conformational in nature, and the primary difference between the two polymorphs lies in the dihedral angle, θ, between the two naphthyl rings linked by a C−C single bond. A number of X-ray crystallographic studies[23−26] have established that one form has θ = 68.6° (Figure 1a), whereas the other form has θ = 103.1° (Figure 1b). The former "cisoid" form, also previously called a low-melting form (mp 145 °C), is a monoclinic (space group $C2/c$) crystal and the

Received: November 6, 2013
Revised: January 9, 2014
Published: January 13, 2014

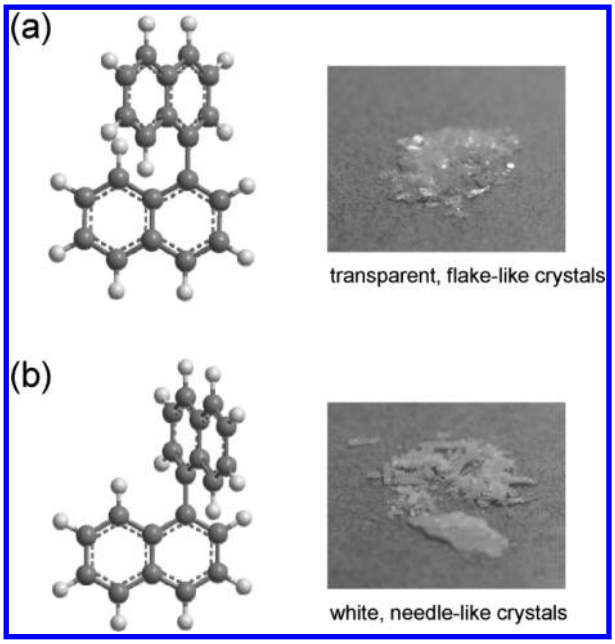

Figure 1. Molecular structures and photographs of typical crystals of the cisoid (a) and transoid (b) forms of BN.

latter "transoid" or high-melting form (mp 160 °C) is tetragonal ($P4_12_12$).[25−27]

The most striking characteristic of BN is that the molecule possesses axial chirality due to restricted rotation around the interannular bond. BN has therefore attracted much attention of chemists as a fundamental structural unit of specific chiral ligands used in asymmetric synthesis,[28] including BINAP[29] (2,2′-bis(diphenylphosphino)-1,1′-binaphthyl). This axial chirality is manifested in a different manner in the polymorphs of BN. The cisoid form is a racemate with a unit cell consisting of two *R*-(−)-enantiomers and two *S*-(+)-enantiomers.[25] In contrast, the transoid form is a conglomerate of optically active single crystals with either *R*-(−)- or *S*-(+)-enantiomers in a unit cell.[26,27] Pincock and co-workers[30,31] found that upon heating, the racemic cisoid form transforms to the chiral transoid form, and described the process as a solid-state resolution. Following their work, Kress et al.[27] re-examined this thermally induced transformation of BN single crystals and concluded that the dominant reaction pathway, at least under their experimental conditions, is a solid−vapor−solid process (involving sublimation) rather than a solid−solid process. Yet another study was conducted by Sainz-Díaz and co-workers,[32] which favored a solid−solid transformation mechanism as had been proposed by Wilson and Pincock.[31] Furthermore, they hypothesized that the cisoid form became a disordered or glassy state before transforming to the transoid form.

In the present work, we shed new light on this controversial mechanism of the polymorphic transformation of BN by looking into LF Raman spectra of microcrystalline BN measured with increasing temperature. We found that the cisoid and transoid forms have markedly different LF Raman spectral profiles that arise predominantly from lattice vibrations. Changes in those spectra during the transformation allow us to gain a molecular picture of the process and infer its mechanism. We demonstrate that the ultralow-frequency Raman spectroscopy presented here offers a fast, molecular-specific tool for tracking phase transitions in various molecular crystals in situ that should be complementary to X-ray diffraction and calorimetry approaches.[33]

EXPERIMENTAL SECTION

Sample Preparation. Powder 1,1′-binaphthyl (98% pure), which was dominated by the cisoid form, was purchased from Tokyo Chemical Industry. To remove impurities and suppress fluorescence that possibly interferes with Raman measurements, the powder sample was first subjected to silica gel column chromatography with *n*-hexane as the eluent. The sample so purified was then used for preparation of cisoid and transoid crystals (Supporting Information, SI, Figure S1) according to a procedure similar to previous reports.[18,32] A 0.35-g portion of the column chromatographically purified BN was placed in a flask and heated up to 180 °C. The melt was kept at this temperature for 15 min, ensuring complete racemization of the sample. After the racemization process, the melt was slowly cooled down to room temperature over 4 h and allowed to recrystallize. Transparent, flake-like cisoid crystals were found at the top of the flask, which formed via evaporation and subsequent recrystallization.[27] White, needle-like transoid crystals were found at the bottom of the container.

Thermal Analysis. To measure the melting points of the two crystal forms, differential scanning calorimetry (DSC) was performed with a DuPont 910 DSC-9000 controller with heating rates of 5, 20, and 45 °C/min for the cisoid form and 5 and 45 °C/min for the transoid form.

Ultralow-Frequency Raman Spectroscopy. A laboratory-built Raman spectrometer equipped with a heating apparatus (SI Figure S2) was used to measure LF (∼5 to 200 cm^{-1}) as well as HF (200−1100 cm^{-1}) Raman spectra at elevated temperatures. The key component in our apparatus to making LF Raman measurements possible is an iodine vapor cell. Because one of the vibronic absorption lines of iodine vapor (∼1 GHz width) coincides with the 514.5 nm line of an Ar^+-ion laser (<40 MHz width), the iodine absorption line can selectively eliminate the laser line. Therefore, the iodine vapor cell works as an extremely narrowband and highly efficient Rayleigh rejection filter.[8,9,11] The cell used in this study was a cylindrical glass cell (Sacher Lasertechnik) with a 2.5 cm diameter and a 10 cm length in which a few milligrams of solid iodine were contained at a high vacuum level (<10^{-3} Torr). The cell was heated to 95 °C and kept at this temperature within ±1 °C by using a rubber heater that wrapped the cell and a thermocouple inserted between the rubber heater and the cell. At 95 °C, the iodine sealed in the cell sublimated to produce iodine vapor. The cell's operating temperature in this work was much lower than the previous work,[11] resulting in a higher transmittance of the cell (>20% in the 0−200 cm^{-1} region with 514.5 nm excitation).

The 514.5 nm line of a single-mode Ar^+-ion laser (BeamLok 2060 with Z-Lok option, Spectra Physics) was used as the excitation light. The beam was focused onto the sample sealed in a cylindrical glass capillary with a 1.1−1.2 mm inner diameter and the scattered light was collected at 90° with a camera lens (f = 50 mm, f/1.2; Nikon). The laser power at the sample point was 55 mW throughout the present study. The collected light was focused on a 5-mm aperture so as to block strong reflection from the capillary walls. The collimated light was then passed through the iodine vapor cell operating at 95 °C, which filtered out virtually all Rayleigh scattering. The transmitted light was analyzed by a spectrograph (f = 500 mm, f/6.5; SP-2558, Princeton Instruments) and detected by a back-illuminated,

dx.doi.org/10.1021/jp410941t | J. Phys. Chem. C 2014, 118, 2702−2709

liquid N_2-cooled charge-coupled device (CCD) camera (Spec-10:100B, Princeton Instruments) with 100 × 1340 pixels operating at −120 °C. The entrance slit of the spectrograph was typically set to 50 μm. A 1200 grooves/mm grating was used to cover a broad spectral range from −200 to 1100 cm^{-1} with a spectral resolution of 2.7 cm^{-1}. A 1 s exposure time was used.

To correct spiky artifacts in the raw spectrum that are inevitably caused by the iodine-vapor absorption structures,[34] the transmission spectrum of the white light from a tungsten lamp was measured before and after each Raman measurement. The white light was introduced into the iodine vapor cell with high reproducibility by a motorized flipper mirror. The observed Raman spectrum was divided by the white light spectrum, yielding the intensity-corrected spectrum that is free from the iodine-vapor artifacts. All Raman spectra shown below were subjected to this correction.

The heating apparatus used in the present study was specifically designed for a 90° scattering geometry (SI Figure S2). The sample temperature was raised by heating coils placed inside the box. The sample sealed in a capillary was inserted from a side hole and a thermocouple was placed in the close vicinity of the capillary to monitor the surrounding temperature. The laser beam was incident from the bottom. The scattered light was collected through a large optical window on a side wall of the heating apparatus.

RESULTS AND DISCUSSION

Raman Spectra of the Two Polymorphs of BN. We first measured the Raman spectra in the −200−1100 cm^{-1} region of the cisoid and transoid forms of the purified microcrystalline BN at room temperature (Figure 2). The 98% pure sample showed strong fluorescence background, but the purified samples did not. The HF region (200−1100 cm^{-1}), in which intramolecular (internal) vibrations are usually observed, is much alike between the cisoid (Figure 2a) and transoid (Figure 2b) forms. The most notable difference can be found in a pair of the Raman bands at 510 and 532 cm^{-1}. The intensity ratio of the 510 cm^{-1} band to the 532 cm^{-1} band, I_{510}/I_{532}, is ∼2 for the cisoid form and ∼1 for the transoid form. This difference in the intensity ratio has been interpreted in terms of a coupling between the two naphthyl groups of BN.[35] Due to the weak coupling, a Raman band at around 520 cm^{-1} in naphthalene splits into a doublet, whose intensity ratio depends on θ.

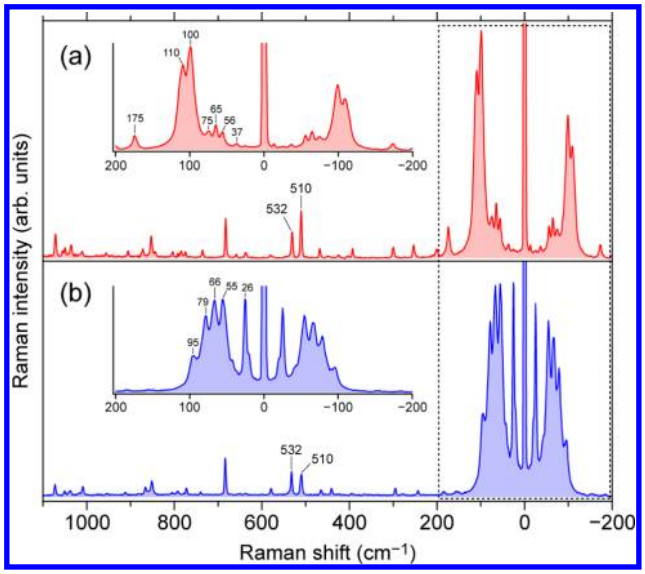

Figure 2. Room-temperature Raman spectra in the −200−1100 cm^{-1} region of the cisoid (a) and transoid (b) forms of purified microcrystalline BN. Insets enlarge the LF part of the spectra.

In comparison with the HF region, the LF region of the Raman spectra exhibits markedly distinct patterns with many intense peaks, which arise predominantly from lattice vibrations. The decent LF Raman spectra in both Stokes and anti-Stokes regions (−200−200 cm^{-1}) were simultaneously obtained in as short as 1 s. This is the first observation, to our knowledge, of thorough LF Raman spectra of the two polymorphs of crystalline BN. The importance of simultaneously measuring not only the Stokes side, but also the anti-Stokes side cannot be overemphasized because it allows us to determine the absolute temperature of the molecule from the Stokes/anti-Stokes intensity ratio of a given Raman band. It also helps to confirm whether a marginal LF signature that is observed in the Stokes region is an artifact (e.g., one caused by iodine vapor) or a real Raman band; if that peak is an artifact, it would not accompany its counterpart in the anti-Stokes region.

The LF Raman spectrum of the cisoid form (the inset in Figure 2a) is dominated by Raman bands at 100 and 110 cm^{-1}. These bands are about an order of magnitude more intense than the HF Raman bands. In addition to the two prominent peaks, we see several minor (but comparable to HF) bands at 37, 56, 65, 75, and 175 cm^{-1} in the cisoid spectrum. In contrast, the transoid form (the inset in Figure 2b) shows almost equally intense Raman bands peaking at 26, 55, 66, 79, and 95 cm^{-1}. By using these Raman bands characteristic of each polymorph, we are able to track the polymorphic transformation of BN with high chemical specificity.

There are 9 (= 6 × 2 − 3) and 21 (= 6 × 4 − 3) optical lattice modes in the cisoid and transoid crystals, respectively. The crystallographic unit cell of both forms contains four BN molecules (i.e., $Z = 4$).[25−27] However, the number of molecules per Bravais cell[36,37] for the cisoid form having a base-centered lattice is two and not four, so that the cisoid form has only 9 lattice modes. Out of 9 and 21 optical lattice modes, group theoretical analysis[36] predicts 6 ($3A_g + 3B_g$) and 11 ($2A_1 + 4B_1 + 2B_2 + 3E$) Raman-active vibrations, respectively. The former agrees well with the number of peaks observed in the cisoid Raman spectrum below 200 cm^{-1} (Figure 2a). The apparent discrepancy between theory and experiment in the number of lattice Raman bands for the transoid form is likely to result from the fact that some of the 11 modes are only of weak intensity and are not fully resolved under the present polarization and temperature conditions. The Raman spectrum of the transoid form below 100 cm^{-1} indeed exhibits a higher baseline and more overlapping bands (Figure 2b) than that of the cisoid form.

It will be interesting to compare the LF Raman spectrum of the cisoid form of BN with that of biphenyl, the simplest biaryl compound. Like the cisoid form of BN, crystalline biphenyl is also monoclinic (space group $P2_1/a$) with unit cell consisting of two biphenyl molecules ($Z = 2$).[38] But crystalline biphenyl at room temperature shows quite a different LF Raman spectrum from the cisoid form of BN, with peaks at 42 (B_g), 54 (A_g), and 88 (A_g) cm^{-1}.[39] One possible reason for the spectral dissimilarity is the distinct molecular conformations in the respective crystals; the biphenyl molecule is planar, whereas the BN molecule is twisted. The comparison between BN and

dx.doi.org/10.1021/jp410941t | J. Phys. Chem. C 2014, 118, 2702−2709

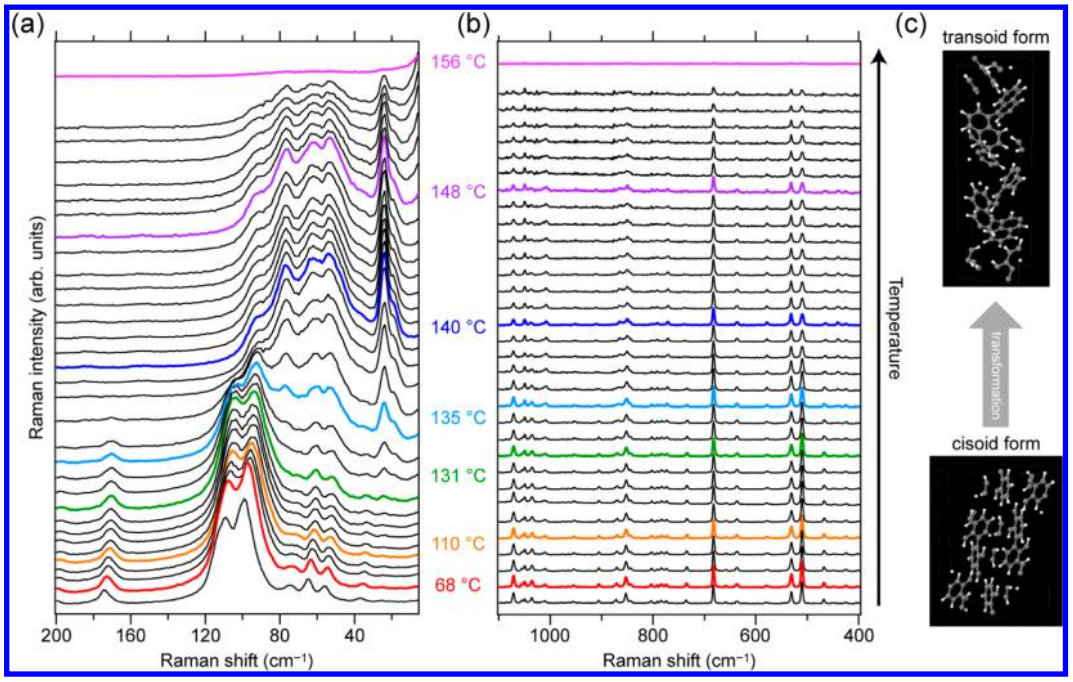

Figure 3. In situ Raman tracking of the cisoid → transoid transformation of microcrystalline BN. (a,b) LF (a) and HF (b) regions of the representative Raman spectra recorded at probe (thermocouple) temperatures of 24, 68, 88, 98, 110, 120, 124, 126, 128, 131, 133, 134, 135, 136, 137, 138, 139, 140, 141, 142, 143, 144, 145, 146, 147, 148, 149, 150, 151, 152, 153, 154, and 156 °C (from bottom to top). The spectra at 68, 110, 131, 135, 140, 148, and 156 °C are highlighted by different colors and they are discussed in detail in text. Note that although only the Stokes region is shown in part a for clarity, the anti-Stokes region was also recorded in our experiment. (c) Illustration of the molecular packing in unit cells of the cisoid and transoid forms of BN.

biphenyl provides more significant insight in relation to the transformation mechanism, as discussed later in this section.

In Situ Tracking of the Transformation Process. Prior to temperature-dependent Raman studies, we performed DSC measurements of the cisoid and transoid crystals with different heating rates (SI Figure S3). The DSC profile of the cisoid form obtained with a sufficiently small heating rate of 5 °C/min (blue trace in SI Figure S3a) shows two endothermic peaks at 146 and 160 °C. The former corresponds to the melting point of the cisoid form and the latter to that of the transoid form. The melting points determined here agree with the literature.[24,27,31] A small exothermic peak observed at 149 °C appears to overlap with the endothermic peak at 146 °C. This profile indicates that the melting of the cisoid form occurs concomitantly with its transformation to the transoid form.[32] As the heating rate increases, the peak at 146 °C gets broadened and shifts to 148 °C with a 20 °C/min heating rate (green trace in SI Figure S3a) and to 152 °C with a 45 °C/min heating rate (red trace in SI Figure S3a). It follows from this finding that, to be able to observe the transformation process, slow heating must be employed. In the DSC curve of the transoid form (SI Figure S3b), only one peak representing its melting is observed and shows a similar trend to the cisoid form as the heating rate is increased.

We now turn to the results of LF Raman measurements. Figure 3 displays representative LF Raman spectra of the cisoid crystals (Figure 3a) measured with increasing the temperature from ambient to 156 °C, together with the corresponding HF spectra (Figure 3b). Also shown in this figure is the molecular packing in unit cells of the two crystal forms of BN (Figure 3c). As confirmed by the DSC experiment discussed above, the sample was heated very slowly with a 3 °C/min heating rate. When the temperature reached the desired value, we waited for 1 min before starting Raman spectral acquisition so that thermal equilibrium was reached. The temperatures shown in Figure 3a,b are those indicated by the thermocouple. Note that each spectrum in Figure 3 was taken with a 1 s exposure time. This is more than just a time-saving advantage compared to previous LF Raman work;[13] it is a quantum leap in methodology because it will extend the applicability of the Raman method to studies of fast phase transitions.

It is clear from Figure 3a that as the temperature increases, the LF Raman spectral pattern varies from the cisoid-form spectrum to the transoid-form spectrum. At 68 and 110 °C, for example, the spectrum exhibits only Raman bands that are ascribed to the cisoid form. However, at 131 °C, a weak band at 26 cm^{-1}, which is a marker band of the transoid form, is already recognizable. In the 135 °C spectrum, the 26 cm^{-1} band becomes more prominent, but the cisoid Raman bands still remain. They completely decay away by 140 °C and the transoid bands dominate the spectrum. The spectrum at 156 °C represents the melt of BN, which no longer shows intense lattice vibrations. It also has a very broad Rayleigh wing typical of liquids. Such a drastic change in spectral pattern is not observed in the HF region (Figure 3b). As described above, only the relative intensity of the 510 and 532 cm^{-1} bands changes significantly with increasing temperature. From these results, we can conclude that the LF Raman bands more sharply reflect the structural change associated with the transformation from the cisoid to the transoid form (see Figure 3c for the unit-cell structures of the two polymorphs) than the HF bands.

Temperature Dependence of Peak Positions and Intensities. To extract quantitative information on the temperature dependence of peak positions and intensities of several cisoid and transoid marker bands, we carried out fitting analysis of the LF Raman spectra (−200 to 200 cm^{-1}) and of

dx.doi.org/10.1021/jp410941t | J. Phys. Chem. C 2014, 118, 2702−2709

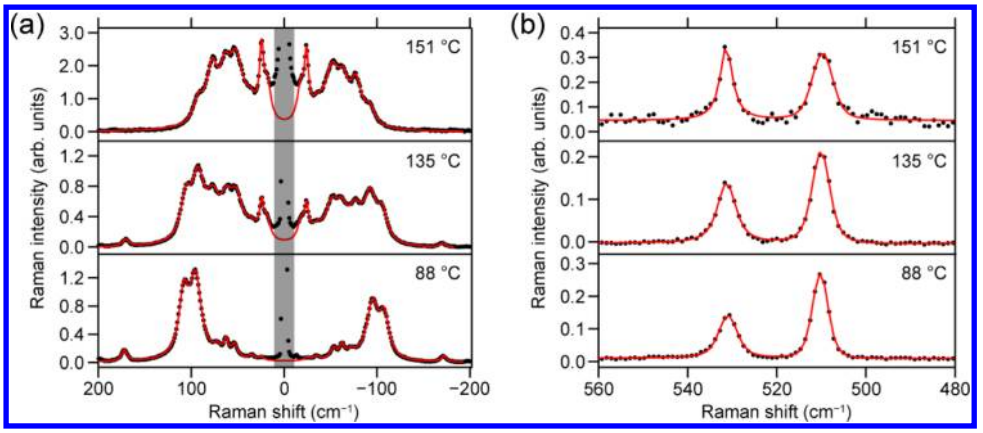

Figure 4. Fitted results of LF (a) and HF (b) Raman spectra at 88, 135, and 151 °C. Black dots represent the normalized experimental spectra and red curves represent best fits to eq 1 (a) and a superposition of two Voigt functions (b). The shaded area was not fitted because of considerable interference with Rayleigh scattering.

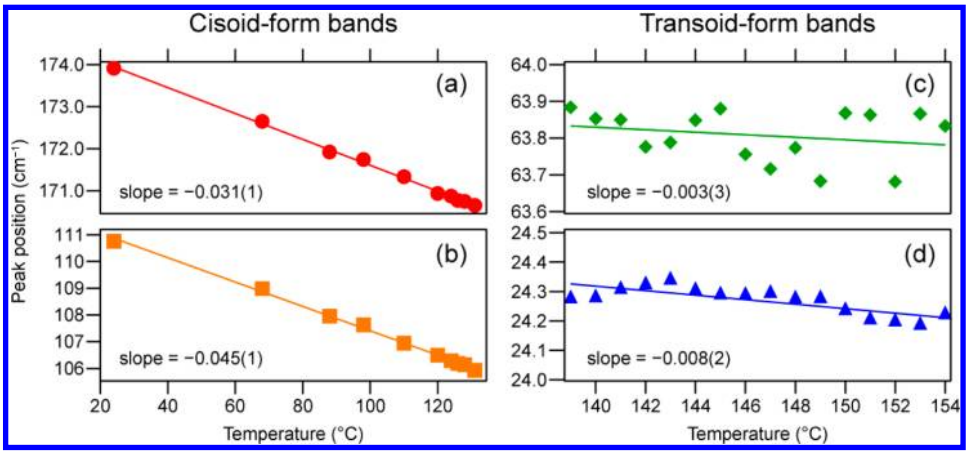

Figure 5. Peak positions of the cisoid (a,b) and transoid (c,d) LF Raman bands versus temperature. Solid lines represent best fits to a linear function, and the slope so obtained is also shown in each panel.

the pair of the 510 and 532 cm^{-1} bands. To take into account intensity fluctuations due to volume changes associated with the melting, we normalized all of the spectra by using the most intense intramolecular vibrational band at 683 cm^{-1} before fitting.

The fitting function used for the LF spectra has the following form:

$$f(\tilde{\nu}) = y_0 + \sum_i \left[\frac{A_i \Gamma_i}{(\tilde{\nu} - \tilde{\nu}_i)^2 + \Gamma_i^2} + \frac{A_i \Gamma_i}{(\tilde{\nu} + \tilde{\nu}_i)^2 + \Gamma_i^2} \right] \times [1 + \exp(-hc\tilde{\nu}/k_B T)]^{-1} \times (\tilde{\nu}_0 - \tilde{\nu})^3 \quad (1)$$

where y_0 is a constant offset of the spectrum, c is the speed of light, h is Planck's constant, k_B is the Boltzmann constant, T is absolute temperature, $\tilde{\nu}_0$ is the absolute wavenumber of the excitation laser, and $\tilde{\nu}$ is the Raman shift. The function in the square brackets in eq 1 represents a sum of two Lorentzian functions for the Stokes and anti-Stokes bands, which are symmetric with respect to $\tilde{\nu} = 0$. Parameters A_i, Γ_i, and $\tilde{\nu}_i$ (>0) denote peak area, bandwidth, and peak position, respectively, of the ith band. Here we assume that the Stokes spectrum below 200 cm^{-1} is composed of a maximum of 9 bands, so the summation over i runs from 1 to 9. We also assume temperature T to be independent of the vibrational mode; that is, we used a common value of T for all of the 9 bands at a given temperature. In fitting the 510 and 532 cm^{-1} bands, we used a sum of two Voigt functions instead of Lorentzian functions, solely for better estimation of the integrated area.

Typical fitted results are shown in Figure 4a for the LF region and in Figure 4b for the 510/532 cm^{-1} band pair. The region between −15 and 15 cm^{-1} (see the shaded area in Figure 4a) is so severely interfered with Rayleigh scattering that it was masked during the fitting. In both cases, the experimental spectra are well reproduced by the fitted curves. The most important parameters that have been determined through the above fitting analysis are temperature, peak position, and peak intensity.

Let us first consider the temperature parameter. The estimated temperature of BN molecules, T, is found to systematically deviate by ~20 K from the temperature probed with a thermocouple (SI Figure S4). Various factors can contribute to making this deviation. The probe temperature may intrinsically be different from the molecular temperature, because the thermocouple only detects the environment temperature outside, although very near, the capillary. Furthermore, accurate temperature determination using the Stokes/anti-Stokes Raman intensity ratio is practically very difficult due to an exponential dependence of the ratio on temperature ($\propto \exp(-hc\tilde{\nu}_i/k_B T)$). Unless some special technique for sensitivity calibration of the spectrometer is employed, such as using the pure rotational Raman spectrum of

dx.doi.org/10.1021/jp410941t | J. Phys. Chem. C 2014, 118, 2702−2709

D_2 as intensity standards,[40] the temperature estimated from the Stokes/anti-Stokes Raman intensity ratio would contain large errors. However, these factors all ought to be systematic. Therefore, we can at least say that the present fitting is valid in the sense that the discrepancy between the estimated and probe temperatures is nearly constant (~20 K) over the wide temperature range studied.

The temperature dependence of the peak positions of the cisoid and transoid Raman bands (Figure 5) provides qualitative insight into intermolecular interactions in the two polymorphs. All of the bands are found to red-shift almost linearly. The cisoid bands (Figure 5a,b) show larger peak shifts (i.e., larger negative slopes obtained with linear fitting) than the transoid bands (Figure 5c,d). It is generally accepted that the peak shift is related to thermal expansion of crystal lattices, so the smaller peak shift observed for the transoid bands suggests stronger intermolecular interactions in the transoid form than in the cisoid form. The molecular arrangements in unit cells of the two polymorphs determined by X-ray diffraction[25−27,32] are consistent with this interpretation. In both forms, the dominant intermolecular interaction is thought to be the CH/π interaction.[41] In the transoid lattice, BN molecules stack in a parallel manner via the CH/π interaction, whereas in the cisoid lattice they form a kind of layer structure and the CH/π interaction between adjacent layers would be relatively weak, resulting in the greater peak shifts.

We finally look into the peak intensity changes with temperature, which reveal molecular details of the transformation process. Figure 6 compares the temperature dependence of the peak (area) intensity plotted against temperature, of the cisoid Raman bands at 175 and 110 cm^{-1} and transoid bands at 66 and 26 cm^{-1}, together with the temperature dependence of the intramolecular band intensity ratio I_{510}/I_{532} and the intensity of another intramolecular band at 300 cm^{-1} (see Figure 2). Here we focus on the behaviors of these bands in the temperature range where the cisoid → transoid transformation occurs (i.e., 120−152 °C). The cisoid bands (Figure 6a,b) start to decline around 133 °C, which represents the onset of the transformation under the present experimental conditions, and virtually simultaneously the transoid bands (Figure 6c,d) emerge and keep growing. At temperatures higher than 140 °C, the cisoid bands disappear, and the intensities of the transoid bands reach a plateau, indicating complete transformation of the cisoid form into the transoid form.

A similar behavior can be seen in the temperature dependence of I_{510}/I_{532} (Figure 6e) because the ratio is associated with the dihedral angle θ (ref 35) and hence the relative abundance of the two polymorphs. However, other than specific pairs of Raman bands like the 510 and 532 cm^{-1} bands, intramolecular vibrational bands are generally silent on crystal structure changes. As shown in Figure 6f, the intensity of the intramolecular Raman band at 300 cm^{-1} remains constant over the whole temperature range of interest within experimental uncertainties. This result also confirms the validity of the normalization procedure we adopted, which uses another intramolecular band at 683 cm^{-1}.

Transformation Mechanism. We infer from the presented LF Raman results (Figures 3 and 6) that the polymorphic transformation of BN occurs predominantly in the solid state under the present conditions. As shown in Figure 6a−d, the transoid bands show up concomitantly with the decrease of the cisoid bands. In addition, the resulting transoid bands are as

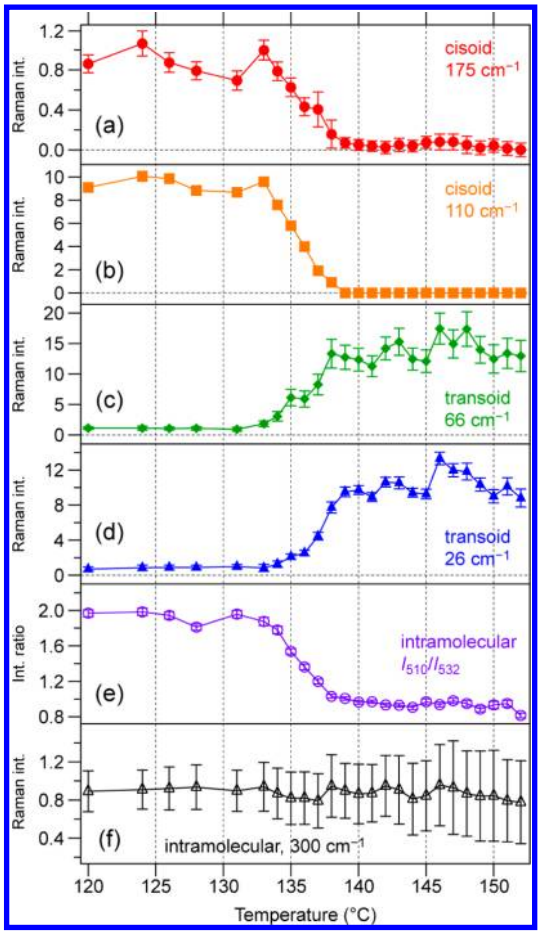

Figure 6. Temperature-dependent changes in LF and HF Raman band intensity during the polymorphic transformation of BN. (a,b) Cisoid bands at 175 (a) and 110 (b) cm^{-1}. (c,d) Transoid bands at 66 and 26 cm^{-1}. (e) Intensity ratio of the intramolecular Raman bands at 510 and 532 cm^{-1}. (f) Intramolecular Raman band at 300 cm^{-1}. Error bars represent fitting errors.

intense as the cisoid bands (see Figure 3a). It is therefore unlikely that the major channel for the transformation involves sublimation of BN and subsequent recrystallization, which would require many hours to produce an amount of transoid crystals comparable to the original cisoid crystals. Although this solid−vapor−solid process argued by Kress et al.[27] may contribute to some extent to the transformation observed in the present study, it is a direct conversion that the majority of BN microcrystals undergoes. In our experiment, the transformation commenced at a much lower temperature (~133 °C) than the reported melting point of the cisoid form. This observation is in line with the phase diagram of BN proposed by Wilson and Pincock.[31] They showed that an equilibrium solid−solid phase transition point exists at ~76 °C in the phase diagram and that above this temperature, the transoid form is more stable relative to the cisoid form, thus leading to the transformation.

More importantly, the LF Raman spectra between 133 and 140 °C (Figure 3a), where the transformation occurs, do not show any bands that are attributable to neither the cisoid nor the transoid BN. In other words, those Raman spectra can be accounted for solely by the two authentic polymorphs. This finding strongly suggests that the cisoid form transforms into the transoid form directly without formation of a disordered or

dx.doi.org/10.1021/jp410941t | J. Phys. Chem. C 2014, 118, 2702−2709

glassy solid[32] that could have a different dihedral angle θ from both cisoid (68.6°) and transoid forms (103.1°). Such information is never obtainable if one focuses only on the I_{510}/I_{532} ratio in the HF region.

How, from the point of view of physics, does the change of structure occur during the cisoid to transoid transformation, a kind of structural phase transition? It is customary to characterize structural phase transitions by two limiting cases: (i) the displacive transition, where only small displacements in the lattice positions of atoms or molecules are involved and (ii) the order−disorder transition, which involves the change in ordering of atoms or molecules.[42] Classification of structural phase transitions into these two limiting cases can be understood in terms of double-well intramolecular potentials, $V(Q)$, for a specific spatial coordinate Q (torsional angle in the BN case) in the crystal,

$$V(Q) = aQ^2 + bQ^4 \quad (2)$$

with $a < 0$ and $b > 0$. When the energy difference between the maximum and two minima of the potential, ΔE, is much smaller than thermal energy $k_B T_c$ (where T_c is the transition temperature), i.e., $\Delta E \ll k_B T_c$, the phase transition would be of the displacive type. In contrast, when $\Delta E \gg k_B T_c$, the phase transition would be attributed to the order−disorder type.

Examples of molecular crystals that show displacive transitions include biphenyl.[42,43] While biphenyl molecules are planar in the room-temperature crystal,[38] they take a nonplanar, twisted conformation below ∼40 K. This phase transition has been known to be displacive[43] because of the small barrier of the double-well potential of crystalline biphenyl. Due to the ortho-hydrogen repulsion, the barrier height increases with increasing the number of phenyl rings, leading to switching of transition mechanisms from displacive to order−disorder. As expected, *p*-terphenyl undergoes the order−disorder transition at T_c = 191 K.[43]

In BN, there exists the harsh repulsion of the hydrogen atoms at the 8 and 8′ positions, in addition to the repulsion of the 2- and 2′-hydrogen atoms. It is therefore plausible that the double-well potential barrier in crystalline BN[16] (<22.5 kcal mol^{-1}) is much larger than that in biphenyl[24] (<4 kcal mol^{-1}) and similar to that in *p*-terphenyl, thereby suggesting the order−disorder nature of the polymorphic transformation of BN. An increase in the entropy of the cisoid form upon heating (i.e., disordering) may well lower the free energy and drive the transformation toward the transoid form.[32] It should be noted, however, that due to coupling effects, the structural phase transitions particularly in molecular crystals cannot be attributed exclusively to either one of the two types,[42] and the polymorphic transformation of BN could have a sizable displacive contribution as well.

CONCLUSIONS

Using the LF Raman spectra measured with slow heating, we have clarified the mechanism for the thermally induced transformation of microcrystalline BN. The cisoid form of BN has been found to transform in the solid state directly to the transoid form without forming any intermediate structure to a measurable extent. All BN molecules in the monoclinic structure will change their conformation through the dihedral angle in a cooperative manner and conform to the tetragonal structure. This mechanism seems to differ from that applying to single crystals of BN,[27] in which sublimation might be the main route of the transformation. To further investigate this interesting issue, we need LF measurements under the microscope, which are currently in progress in our laboratory. Our in situ LF Raman tracking is applicable to whatever the system showing phase transitions, including pharmaceutical compounds, liquid crystals, and polymer films.

ASSOCIATED CONTENT

Supporting Information

Scheme of sample preparation (Figure S1); low-frequency Raman spectrometer (Figure S2); results of differential scanning calorimetry measurements (Figure S3); and probe temperature vs estimated temperature (Figure S4). This material is available free of charge via the Internet at http://pubs.acs.org.

AUTHOR INFORMATION

Corresponding Author

*E-mail: shigeto@mail.nctu.edu.tw.

Notes

The authors declare no competing financial interest.

ACKNOWLEDGMENTS

We thank Professor Henryk A. Witek for helpful discussions on low-frequency band assignments and Dr. Hajime Okajima for his advice on the low-frequency Raman spectrometer. S.S. acknowledges the Aiming for the Top University plan of the National Chiao Tung University for financial support.

REFERENCES

(1) Morris, K. R.; Griesser, U. J.; Echkhardt, C. J.; Stowell, J. G. Theoretical Approaches to Physical Transformations of Active Pharmaceutical Ingredients during Manufacturing Processes. *Adv. Drug Delivery Rev.* **2001**, *48*, 91−114.

(2) Datta, S.; Grant, D. J. W. Crystal Structures of Drugs: Advances in Determination, Prediction, and Engineering. *Nat. Rev. Drug Discov.* **2004**, *3*, 42−57.

(3) Moulton, B.; Zaworotko, M. J. From Molecules to Crystal Engineering: Supramolecular Isomerism and Polymorphism in Network Solids. *Chem. Rev.* **2001**, *101*, 1629−1658.

(4) Desiraju, G. R. Crystal Engineering: A Holistic View. *Angew. Chem., Int. Ed.* **2007**, *46*, 8342−8356.

(5) Desiraju, G. R. Polymorphism: The Same and Not Quite the Same. *Cryst. Growth Des.* **2008**, *8*, 3−5.

(6) Hirsch, A. The Era of Carbon Allotropes. *Nat. Mater.* **2010**, *9*, 868−871.

(7) Nangia, A. Conformational Polymorphism in Organic Crystals. *Acc. Chem. Res.* **2008**, *41*, 595−604.

(8) Devlin, G. E.; Davis, J. L.; Chase, L.; Gerschwind, S. Absorption of Unshifted Scattered Light by a Molecular I_2 Filter in Brillouin and Raman Scattering. *Appl. Phys. Lett.* **1971**, *19*, 138−141.

(9) Wall, K. F.; Chang, R. K. I_2-Vapor Notch Filter with Optical Multichannel Detection of Low-Frequency-Shift Inelastic Scattering from Surface-Enhanced Raman-Scattering Active Electrodes. *Opt. Lett.* **1986**, *11*, 493−495.

(10) Wall, K. F.; Chang, R. K. Separation of the Low-Frequency Mode from the Inelastic Continuum Scattering of a SERS Active Electrode. *Chem. Phys. Lett.* **1986**, *129*, 144−148.

(11) Okajima, H.; Hamaguchi, H. Fast Low Frequency (Down to 10 cm^{-1}) Multichannel Raman Spectroscopy Using an Iodine Vapor Filter. *Appl. Spectrosc.* **2009**, *63*, 958−960.

(12) Okajima, H.; Hamaguchi, H. Unusually Long trans/gauche Conformational Equilibrium Time during the Melting Process of BmimCl, a Prototype Ionic Liquid. *Chem. Lett.* **2011**, *40*, 1308−1309.

(13) Hédoux, A.; Decroix, A.-A.; Guinet, Y.; Paccou, L.; Derollez, P.; Descamps, M. Low- and High-Frequency Raman Investigations on Caffeine: Polymorphism, Disorder and Phase Transition. *J. Phys. Chem. B* **2011**, *115*, 5746−5753.
(14) Friedel, R. A.; Orchin, M.; Reggel, L. Steric Hindrance and Short Wave Length Bands in the Ultraviolet Spectra of Some Naphthalene and Diphenyl Derivatives. *J. Am. Chem. Soc.* **1948**, *70*, 199−204.
(15) Hochstrasser, R. M. The Effect of Intramolecular Twisting on the Emission Spectra of Hindered Aromatic Molecules. *Can. J. Chem.* **1961**, *39*, 459−470.
(16) Cooke, A. S.; Harris, M. M. Ground-State Strain and Other Factors Influencing Optical Stability in the 1,1′-Binaphthyl Series. *J. Chem. Soc. (Resumed)* **1963**, 2365−2373.
(17) Shank, C. V.; Ippen, E. P.; Teschke, O.; Eisenthal, K. B. Picosecond Dynamics of Conformational Changes in 1,1′-Binaphthyl. *J. Chem. Phys.* **1978**, *67*, 5547−5551.
(18) Kondepudi, D. K.; Laudadio, J.; Asakura, K. Chiral Symmetry Breaking in Stirred Crystallization of 1,1′-Binaphthyl Melt. *J. Am. Chem. Soc.* **1999**, *121*, 1448−1451.
(19) Fujiyoshi, S.; Takeuchi, S.; Tahara, T. Time-Resolved Impulsive Stimulated Raman Studies of 1,1′-Binaphthyl in the Excited State: Low-Frequency Vibrations and Conformational Relaxation. *J. Phys. Chem. A* **2004**, *108*, 5938−5943.
(20) Zhang, F.; Bacskay, G. B.; Kable, S. H. Quantum Chemical Determination of the Equilibrium Geometries and Harmonic Vibrational Frequencies of 1,1′-, 1,2′-, and 2,2′-Binaphthyl in Their Ground and Excited (^1L_a) Electronic States. *J. Phys. Chem. A* **2004**, *108*, 172−184.
(21) Liégeois, V. A Vibrational Raman Optical Activity Study of 1,1′-Binaphthyl Derivatives. *ChemPhysChem* **2009**, *10*, 2017−2025.
(22) Jonkman, H. T.; Wiersma, D. A. Spectroscopic Study of Conformational Dynamics of 1,1′-Binaphthyl in a Jet. *J. Chem. Phys.* **1984**, *81*, 1573−1582.
(23) Brown, W. A. C.; Trotter, J.; Robertson, J. M. X-Ray Study of Crystals Isolated during the Synthesis of 1,12-*o*-Phenyleneperylene. *Proc. Chem. Soc.* **1961**, 115−116.
(24) Badar, Y.; Ling, C. C. K.; Cooke, A. S.; Harris, M. M. Two Crystalline Modifications of 1,1′-Binaphthyl. *J. Chem. Soc.* **1965**, 1543−1544.
(25) Kerr, K. A.; Robertson, J. M. Crystal and Molecular Structure of 1,1′-Binaphthyl. *J. Chem. Soc. B* **1969**, 1146−1149.
(26) Kuroda, R.; Mason, S. F. The Crystal and Molecular Structure of *R*-(−)-1,1′-Binaphthyl: The Conformational Isomerism and a Comparison of the Chiral with the Racemic Packing Mode. *J. Chem. Soc. Perkin Trans. 2* **1981**, 167−170.
(27) Kress, R. B.; Duesler, E. N.; Etter, M. C.; Paul, I. C.; Curtin, D. Y. Solid-State Resolution of Binaphthyl: Crystal and Molecular Structures of the Chiral (A) Form and Racemic (B) Form and the Study of the Rearrangement of Single Crystals. Requirements for Development of Hemihedral Faces for Enantiomer Identification. *J. Am. Chem. Soc.* **1980**, *102*, 7709−7714.
(28) Pu, L. 1,1′-Binaphthyl Dimers, Oligomers, and Polymers: Molecular Recognition, Asymmetric Catalysis, and New Materials. *Chem. Rev.* **1998**, *98*, 2405−2494.
(29) Noyori, R.; Takaya, H. BINAP: An Efficient Chiral Element for Asymmetric Catalysis. *Acc. Chem. Res.* **1990**, *23*, 345−350.
(30) Pincock, R. E.; Perkins, R. R.; Ma, A. S.; Wilson, K. R. Probability Distribution of Enantiomorphous Forms in Spontaneous Generation of Optically Active Substances. *Science* **1971**, *174*, 1018−1020.
(31) Wilson, K. R.; Pincock, R. E. Thermally Induced Resolution of Racemic 1,1′-Binaphthyl in the Solid State. *J. Am. Chem. Soc.* **1975**, *97*, 1474−1478.
(32) Sainz-Díaz, C. I.; Martín-Islán, A. P.; Cartwright, J. H. E. Chiral Symmetry Breaking and Polymorphism in 1,1′-Binaphthyl Melt Crystallization. *J. Phys. Chem. B* **2005**, *109*, 18758−18764.
(33) Kato, T.; Okamoto, I.; Masu, H.; Katagiri, K.; Tominaga, M.; Yamaguchi, K.; Kagechika, H.; Azumaya, I. Polymorphism and Pseudopolymorphism of an Aromatic Amide: Spontaneous Resolution and Crystal-to-Crystal Phase Transition. *Cryst. Growth Des.* **2008**, *8*, 3871−3877.
(34) Scherer, J. R. Removal of I_2 Absorption Lines from 514-nm Excited Raman Spectra. *Appl. Opt.* **1978**, *17*, 1621−1623.
(35) Lacey, A. R.; Craven, F. J. A Preliminary Study of the Conformation of 1,1′-Binaphthyl in Solution by Raman Spectroscopy. *Chem. Phys. Lett.* **1986**, *126*, 588−592.
(36) Fateley, W. G.; McDevitt, N. T.; Bentley, F. F. Infrared and Raman Selection Rules for Lattice Vibrations: The Correlation Method. *Appl. Spectrosc.* **1971**, *25*, 155−173.
(37) Nakamoto, K. *Infrared and Raman Spectra of Inorganic and Coordination Compounds. Part A: Theory and Applications in Inorganic Chemistry*, 5th ed.; John Wiley & Sons: New York, 1997.
(38) Trotter, J. The Crystal and Molecular Structure of Biphenyl. *Acta Crystallogr.* **1961**, *14*, 1135−1140.
(39) Burgos, E.; Bonadeo, H.; D'Alessio, E. Vibrational Calculations on the Biphenyl Crystal: The Mixing between Low Frequency Internal and Lattice Modes. *J. Chem. Phys.* **1976**, *65*, 2460−2466.
(40) Hamaguchi, H.; Harada, I.; Shimanouchi, T. Sensitivity Calibration of a Raman Spectrometer Using the Rotational Raman Spectra of Deuterium. *Chem. Lett.* **1974**, 1405−1410.
(41) Nishio, M.; Hirota, M.; Umezawa, Y. *The CH/π Interaction: Evidence, Nature, and Consequences*; Wiley-VCH: New York, 1998.
(42) *Vibrational Spectroscopy of Phase Transitions*; Iqbal, Z., Owens, F. J., Eds.; Academic Press: Orlando, 1984.
(43) Cailleau, H.; Baudour, J.-L.; Meinnel, J.; Dworkin, A.; Moussa, F.; Zeyen, C. M. E. Double-Well Potentials and Structural Phase Transitions in Polyphenyls. *Faraday Discuss. Chem. Soc.* **1980**, *69*, 7−17.